Boron distribution in the core of Si nanowire grown by chemical vapor deposition

W. Chen, V.G. Dubrovskii, X.L. Liu, T. Xu, Rodrigue Lardé, J.P. Nys, B. Grandidier, D. Stievenard, G. Patriarche, Philippe Pareige

Boron distribution in the core of Si nanowire grown by chemical vapor deposition

Cite as: J. Appl. Phys. **111**, 094909 (2012); https://doi.org/10.1063/1.4714364
Submitted: 02 February 2012 • Accepted: 08 April 2012 • Published Online: 10 May 2012

Wanghua Chen, Vladimir G. Dubrovskii, Xiaolong Liu, et al.

Boron distribution in the core of Si nanowire grown by chemical vapor deposition

Wanghua Chen,[1] Vladimir G. Dubrovskii,[2,3] Xiaolong Liu,[2,4] Tao Xu,[5] Rodrigue Lardé,[1] Jean Philippe Nys,[5] Bruno Grandidier,[5] Didier Stiévenard,[5] Gilles Patriarche,[6] and Philippe Pareige[1,a)]

[1]*Groupe de Physique des Matériaux, Université et INSA de Rouen, CNRS, UMR 6634, Av. de l'Université, BP 12, 76801 Saint Etienne du Rouvray, France*
[2]*St. Petersburg Academic University, Khlopina 8/3, 194021 St. Petersburg, Russia*
[3]*Ioffe Physical Technical Institute RAS, Politekhnicheskaya 26, 194021 St. Petersburg, Russia*
[4]*State Key Laboratory of Information Photonics and Optical Communications, Beijing University of Posts and Telecommunications P.O. Box 66, Beijing 100876, China*
[5]*Institut d'Electronique, de Microélectronique et de Nanotechnologie, CNRS, UMR 8520, Département ISEN, 41 bd Vauban, 59046 Lille Cedex, France*
[6]*CNRS-Laboratoire de Photonique et de Nanostructures, Route de Nozay, 91460 Marcoussis, France*

(Received 2 February 2012; accepted 8 April 2012; published online 10 May 2012)

The boron dopant distribution in Si nanowires grown by the Au-catalyzed chemical vapor deposition is characterized by laser-assisted atom probe tomography. A convenient and an effective method for performing the atom probe tomography of an individual nanowire is developed. Using this technique, we demonstrate that when Si nanowires are doped with boron at high silane partial pressure, the radial distribution of boron atoms is rather inhomogeneous. Much more boron atoms incorporate at the periphery than in the center, with the concentration increasing by an order of magnitude as the distance from the nanowire axis increases from zero to only 15 nm. A theoretical model is presented that is capable of describing the observed spatial inhomogeneity of boron dopant. We also consider different kinetic pathways of boron incorporation and discuss the values of diffusion length and diffusion coefficients obtained by fitting the experimental data. © *2012 American Institute of Physics*. [http://dx.doi.org/10.1063/1.4714364]

I. INTRODUCTION

Growth and physical properties of Si nanowires (NWs) have been studied extensively in recent years. In view of many potential applications in nanoelectronics, investigations of doping processes in Si NWs have been of major interest.[1–5] Compared to other methods, the chemical vapor deposition (CVD) of Si NWs via the Au-catalyzed vapor-liquid-solid (VLS) mechanism[6] is most advantageous. Indeed, the Au-assisted CVD enables a high growth rate of Si NWs as well as a precise control of doping precursor during growth. Characterization of dopant spatial distribution in individual NWs is very important for understanding the doping mechanisms as well as the resulting electrical properties. Several methods have been used for such characterization, for example, the capacitance-voltage measurement of B-doped Si NW,[7] the Kelvin probe force microscopy of P-doped Si NW,[8] and the atom probe tomography (APT) of P-doped Ge NW.[9] An inhomogeneous dopant distribution in those NWs has been recently found to be a common phenomenon, regardless of NW shape. In particular, Koren and coauthors have demonstrated that the concentration of P atoms in straight Si NWs can decrease by two orders of magnitude from the NW sidewall surface to the core.[8] The authors hypothesized that P atoms could diffuse directly from the vapor phase into the body of Si NW, with an enhanced diffusion coefficient compared to bulk. From their APT investigations, Perea and coauthors have shown that P atoms can migrate into the NW from a conformal deposition layer on the tapered Ge NW sidewalls. An inhomogeneous P distribution in strongly tapered Ge NWs might be due to different dopant incorporation rates on the catalyst surface and the NW sidewalls.[9]

The aim of this work is to investigate the boron distribution in Si NWs grown by the Au-catalyzed CVD via the VLS mechanism. We develop a convenient and an effective method to perform the APT characterization of B-doped Si NWs. Using this technique, we obtain quantitative information on the boron spatial distribution in the 30 nm wide core region and present the radius dependence of the doping profile. A theoretical model is then developed to describe the observed spatial inhomogeneity. We consider possible kinetic pathways of boron incorporation and discuss the values of diffusion length and diffusion coefficients obtained by fitting the experimental data.

II. APT TECHNIQUE

In order to ensure sufficient evaporation field on the apex surface, a specimen analyzed by the APT should have a tip diameter normally smaller than 100 nm. Therefore, a properly manipulated individual Si NW is already an excellent specimen for APT. To the best of our knowledge, only the core region of NW samples can be investigated by the APT, while the important information regarding the outer region and the sidewalls are lost during the analysis.

a)Author to whom correspondence should be addressed. Electronic mail: philippe.pareige@univrouen.fr.

This is well understood since the APT technique uses a projection-based microscope with a planar and limited detector.[10,11] Considering the hemispherical geometry projection, the radius of analyzed NW core, r, can be written as[12]

$$r = R \sin[(m+1)\arctan(R_D/L)], \quad (1)$$

where R is the NW radius, R_D is the radius of detector, m is a dimensionless geometric factor which equals to 0.6, and L is the work distance between sample and detector. In our APT instrumentation (CAMECA LAWATAP), the values of R_D and L amount to 3.85 cm and 9.8 cm, respectively. From Eq. (1), the radius r is estimated as 0.56 R. It can be therefore concluded that the NW surface is missing for the analysis regardless of NW radius when the NW is perpendicular to the detector. Knowing the exact diameter of the NW (by SEM) before analysis and knowing the exact diameter of the analyzed volume are essential for the understanding of the volume reconstruction.

To prepare Si NWs for the APT investigation, several methods have been proposed such as growth on Si micropillars[3,13] and the lift-out method.[14] However, these methods are very time consuming. Here, we have developed a more convenient and an effective sample preparation technique, namely, welding a single Si NW on a supported tip (Fig. 1(a)). The Si NW is first cleaved from its substrate midway between the top and the bottom of the NW, a few micrometers below the Au seed particle, then manipulated, and finally welded directly onto a W tip in the scanning electron microscope—focused ion beam—gas injection system (SEM-FIB-GIS) manipulator workstation. The welding process is realized by GIS in the electron beam-induced deposition (EBID) mode, which is an effective *in situ* nano-scale deposition process (Fig. 1(b)). The specimen analyzed by the APT should have good electrical and mechanical properties. Therefore, (Me_3) MeCpPt and Pt are chosen as the deposition precursor and the solder for reinforcement, respectively. The APT analyzing conditions are set at 80 K with a chamber pressure of about 10^{-10} mbar. The laser is operating in the ultraviolet range (343 nm) with a power of 2.8 mW. This enables an excellent and controlled evaporation rate. By taking the advantage of APT, different elements are detected and viewed in three-dimensional (3D) space.

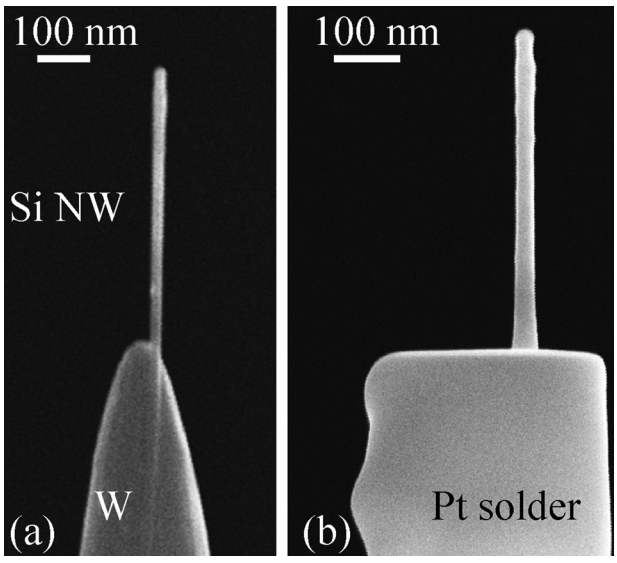

FIG. 1. SEM image of a Si NW welded on a W tip. (a) Before and (b) after Pt deposition by GIS. The bottom end of Si NW is at the top of the specimen.

III. EXPERIMENTAL RESULTS

The Au diffusion from the droplet during growth is known to produce a tapering effect on Si NWs.[15,16] To strongly reduce this effect, our Si NWs are synthesized at a high SiH_4 gas pressure of 0.65 mbar. B_2H_6 is used as the dopant precursor with the fluxes ratio SiH_4:B_2H_6 of 4000:1. The B-doped SiNWs are grown at 500 °C for 20 min.

The Si NWs were first investigated by high resolution transmission electron microscopy (HRTEM) to determine their crystalline structure. For the first 600–1000 nm below the Au droplet, we observe that NWs are covered by Au-rich clusters. Such clusters are caused by the further growth of the NWs from residual silane gas after the interruption of the gas flow in the growth chamber and the subsequent diffusion of gold due to the high-temperature inertia of the chamber. Below this region, the sidewalls are not contaminated by gold clusters, and a thin shell appears as we analyzed the NWs further away from its apex. The shell becomes thicker and thicker towards the cleaved end of the NWs, as lateral growth occurs over a longer time at the bottom of the NWs. In the region of the cleavage that is usually located 6–8 μm below the Au droplet, the typical shell thickness is between 5 and 10 nm as shown in Fig. 2. In contrast to the core, the shell appears polycrystalline (Fig. 2(b)). The defective shell has already been attributed to an overgrown layer that contains a heavy concentration of boron impurities.[17] The high resolution TEM images and dark-field TEM images do not reveal any significant structural change of the shell structure along the NW growth direction, suggesting that the axial dopant concentration in the shell is constant.

In parallel to the TEM analysis, APT characterizations were performed in the region of the cleaved end of the NWs that were also located between 6 and 8 μm from the Au droplet. Figure 3(a) shows the SEM image of the cleaved portion of a Si NW that has been analyzed by APT. This NW cleaved 8 μm below the Au droplet. It has a diameter of 58 nm, but only the cylindrical core with a diameter of 30 nm was probed due to the limitation explained above. Figure 3(b) shows a

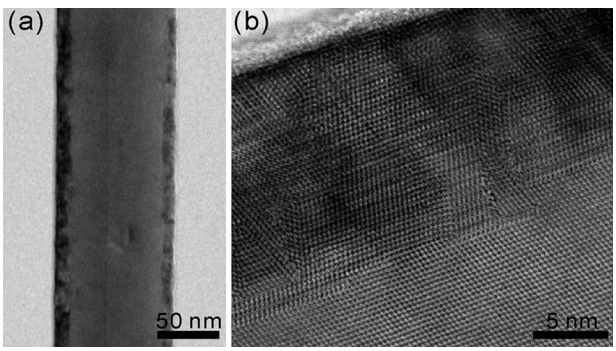

FIG. 2. (a) TEM image of a portion of a Boron-doped Si NW obtained midway between the top and bottom of the NW. (b) HRTEM image of the shell structure.

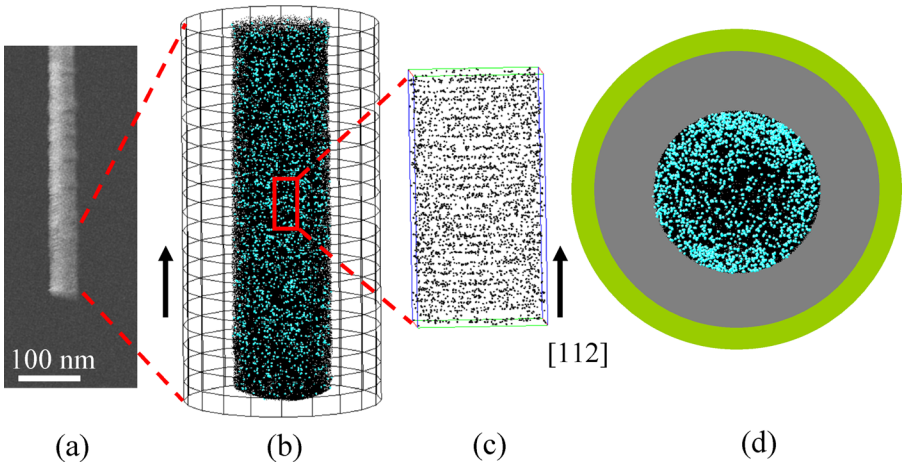

FIG. 3. APT investigation of the core region of an individual B-doped Si NW. (a) SEM image of the cleaved part of the wire that was analyzed. (b) 3D tomographic reconstruction of B atoms (blue dots) and Si atoms (black matrix) in the core of a 58 nm diameter Si NW. The analyzed volume is $30 \times 30 \times 116\,\text{nm}^3$. (c) Enlarged view of the 3D tomographic reconstruction to show the Si inter plane distance of 0.22 ± 0.01 nm. The arrows point in the growth direction. (d) Cross-sectional view of radial B distribution and schematic illustration of the NW radial structure. The grey and green regions represent the part of the Si NW that is not probed and the silica layer, respectively.

3D reconstruction of the core that extends from the cleavage point over 116 nm along the growth axis. The good crystallinity of the NW core is demonstrated from the resolution of the inter-plane distance of 0.22 ± 0.01 nm along the [112] growth direction (Fig. 3(c)), consistent with the HRTEM images of the core. In addition to the Si species, boron is also detected. The concentration of boron impurities establishes at $1 \times 10^{19}\,\text{cm}^{-3}$ in the centre of the Si NW and gradually increases towards the edge of the core.

Before discussing the mechanisms of B incorporation, it is important to verify that the observed non-uniform spatial distribution shown in Fig. 3(d) is not due to atomic surface migration under laser pulses during the APT measurements as it is reported, for example, in Ref. 18. For checking the surface migration effect, Si NWs were synthesized by "top-down" etching of B-doped Si substrate ($1 \times 10^{19}\,\text{cm}^{-3}$) using the Langmuir-Blodgett assembly[19] and were also investigated by APT. SEM images of those NWs are presented in Fig. 4(a). After welding a single NW on a W tip as described above, the NW is polished by annular milling (SEM-FIB) to decrease its initial diameter below 100 nm. The APT investigation conditions are the same as in the previous case. The 3D reconstructions of a portion of Si NW are shown in Figs. 4(b) and 4(c). As seen from Fig. 4, both the axial and the radial B distributions are spatially homogeneous. This homogeneity has also been confirmed numerically by statistical Chi-square test for three different NWs. The mean B concentration is calculated to be $1.1 \pm 0.1 \times 10^{19}\,\text{cm}^{-3}$. This value is of the same order as the initial doping concentration of the Si wafer ($1 \times 10^{19}\,\text{cm}^{-3}$). Therefore, the observed inhomogeneous B distribution in our VLS NWs is not caused by the femtosecond laser illumination of APT but is established during the Au-catalyzed CVD growth.

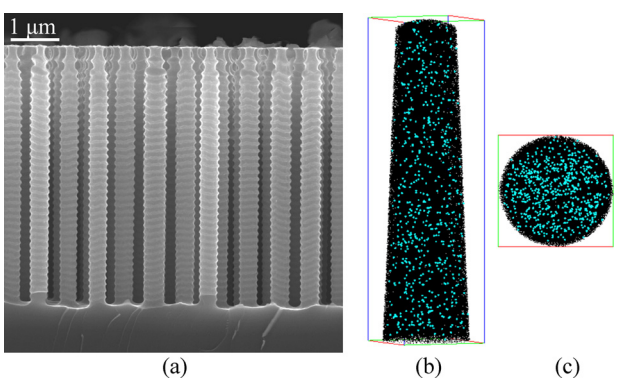

FIG. 4. (a) Side view SEM image of Si NWs fabricated by etching a B-doped Si substrate. (b) Side view and (c) cross-section view of the atomically resolved three-dimensional boron distribution in the core of a Si NW. Boron atoms appear as blue dots, whereas the black matrix represents Si atoms.

IV. MODEL AND DISCUSSION

One can consider three different pathways for the dopant incorporation into a NW, as illustrated in Fig. 5. The first

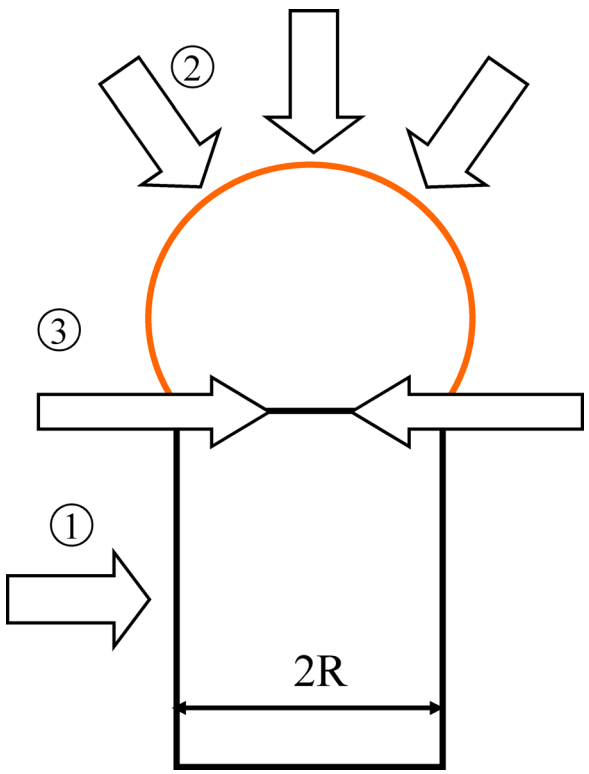

FIG. 5. Schematic illustration of three pathways of dopant incorporation into a VLS NW: (1) VS mechanism; (2) VLS mechanism; (3) ID mechanism.

pathway (arrow 1) corresponds to the direct incorporation from the vapor phase through the NW sidewalls. This is the vapor-solid (VS) incorporation by the solid diffusion, considered previously, for example, in Ref. 8. The second pathway (arrow 2) is the incorporation through the catalyst droplet in the VLS fashion. As discussed in Ref. 9, the dopant profile inside the NW should be governed by the VS incorporation rather than by the VLS-like diffusion because of a higher dissociative chemisorption rate on the NW sidewalls with respect to the droplet surface. The VLS mechanism alone cannot satisfactorily explain the observed spatial inhomogeneity of boron concentration that gradually increases towards the NW sidewalls and is not considered below. In Fig. 5, the third possible pathway is illustrated by arrow 3. This mechanism involves two-dimensional (2D) interfacial diffusion (ID) along the solid-liquid interface between the droplet and the NW.

In the foregoing analysis, we ignore the VLS pathway 2 and consider only the VS or ID mechanisms 1 or 3. Assuming the NW as being a cylinder of radius R, both mechanisms can be described by the two-dimensional non-stationary diffusion equation of the form

$$\frac{\partial C}{\partial t} = \frac{1}{r}\frac{\partial}{\partial r}\left(rD\frac{\partial C}{\partial r}\right). \tag{2}$$

Here, $C(r,t)$ is the radius dependent dopant concentration at time t, r is the distance from the NW axis, and D is the dopant diffusion coefficient.

We now discuss an important issue of selecting the appropriate boundary condition to Eq. (2). The initial and boundary conditions to Eq. (2) are generally given by

$$C(r,t=0)=0, C(r=0,t)<\infty, C(r=R_0,t)=M(t). \tag{3}$$

The initial condition at $t=0$ is obvious. The first boundary condition at $r=0$ yields a finite B concentration at the NW axis. The second boundary condition is usually put at the NW sidewalls ($R_0=R$), with the function M increasing linearly with time: $M=kt$.[4] The solution to Eq. (2) with the boundary conditions given by Eq. (3) is readily obtained in the form

$$C(r,t)=k\left(t-\frac{R^2-r^2}{4D}\right)+\frac{2k}{RD}\sum_{n=1}^{\infty}\exp(-\alpha_n^2 Dt)\frac{J_0(\alpha_n r)}{\alpha_n^3 J_1(\alpha_n R)}. \tag{4}$$

Here, J_k are the Bessel functions of the first kind of the order k and α_n are the roots of the equation $J_0(\alpha_n R)=0$. These roots, along with the corresponding values of $J_1(\alpha_n R)$ and $J_0(\alpha_n r)$, can be found, for example, in Ref. 20. Only the first ten of an infinite set of Bessel function roots are taken into account. This ensures a high accuracy of approximation due to a strong decay of exponential terms of Eq. (4) with increasingα_n.

The boundary condition with $M=kt$ can be justified by considering the surface concentration of boron, c, on the NW sidewalls, driven by the material influx from the vapor phase, J: $dc/dt=J$, yielding $c=Jt$. However, the linear increase with time can be broken by the boron desorption from the sidewalls that should occur at the typical growth temperatures around 500 °C. When the desorption is included, the kinetic equation for c is changed to $dc/dt=J-c/\tau$, with τbeing the effective lifetime on the sidewalls. In this case, the solution is given by $c=J\tau[1-\exp(-t/\tau)]$, showing that, rather than growing infinitely, the surface concentration saturates at a constant value of $J\tau$ at $t\gg\tau$. Therefore, a more reasonable boundary condition at large enough t would be a constant concentration

$$C(r=R_0,t)=C_0=const. \tag{5}$$

With this condition, the solution to Eq. (2) is given by

$$\frac{C(r,t)}{C_0}=1-\frac{2}{R_0}\sum_{n=1}^{\infty}\exp(-\alpha_n^2 Dt)\frac{J_0(\alpha_n r)}{\alpha_n J_1(\alpha_n R_0)}. \tag{6}$$

As already mentioned, our APT characterization is performed within the NW core region of 15 nm radius. The TEM characterization of the NW shows the existence of three different regions: a core radius, a 5–10 nm thick shell with a high concentration of boron impurities, and a 3–4 nm thick SiO_2 layer, yielding the total NW radius of about 29 nm. Therefore, the outermost region in our APT reconstruction (15 nm) is located close to the interface between the core and the overgrown shell. Assuming, in the first approximation, that the boron concentration in the shell is constant, we put the boundary condition given by Eq. (5) at $R_0=15$ nm, with C_0 being equal to the outermost boron concentration measured by APT (7.1×10^{19} cm^{-3}). With this determination made, the fitting of boron concentration profile depends on only one parameter, i.e., the squared effective diffusion length of boron, Dt. Figure 6 shows the profile of the average radial boron distribution measured with APT and theoretical curves obtained from Eq. (6) at different Dt. The best fit is obtained at $Dt=20.25$ nm^2.

If boron incorporates with the VS fashion, time t should be equal to the exposition time of the analyzed section to the

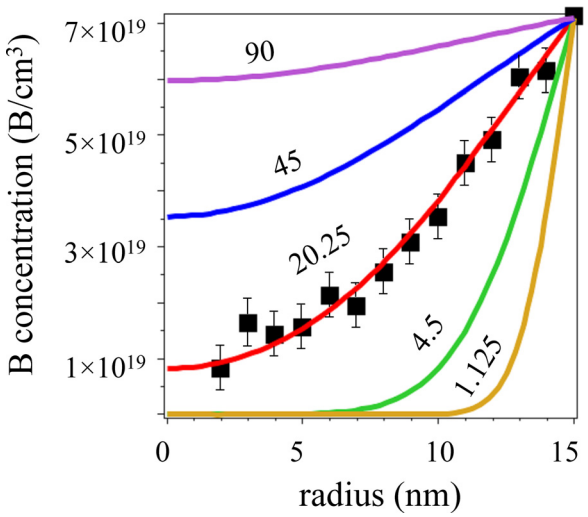

FIG. 6. Measured B concentration (dots) and theoretical concentration profiles (lines) obtained from Eq. (6) at fixed $C_0=7.1\times10^{19}$ cm^{-3}, $R_0=15$ nm, and different Dt (nm^2).

B precursor. The exposure time can be calculated as $t = L/V$, where L is the distance between the cleavage point (the analyzed section) and the Au droplet and V is the NW growth rate. The length L is measured to be 8 μm and V equals 1 μm/min in our CVD experiments, yielding $t = 8$ min, that is supposed to be much longer than τ. As a consequence, the best fit given in Fig. 6 corresponds to $D = 4.22 \times 10^{-16}$ cm^2/s. This value is much larger than the reported bulk diffusivity of B in Si at 500 °C ($\approx 10^{-18}$ cm^2/s).[21] With $D = 10^{-18}$ cm^2/s, the penetration length of B atoms would be only 1 nm, and the VS mechanism could never work in this case. Therefore, the VS incorporation can explain our data only if the boron diffusivity is dramatically enhanced. It has been argued previously that P atoms can diffuse into Ge NWs with an enhanced diffusivity as high as $\approx 10^{-15}$ cm^2/s at 460 °C.[8] As for B atoms in Si NWs, the shell of the NWs has been shown to exhibit defects (see Fig. 2) that could enhance the diffusion of the B impurities. For example, if a supersaturation of Si self-interstitial exists in the shell, it would favor the migration of B-Si interstitial defect complexes that would migrate towards the core and spontaneously break into an interstitial and a substitutional B.[22–24] The solid diffusivity of B could also be enhanced by the elastic stress, an example being the stress-driven diffusion during growth of Stranski-Krastanow quantum dots.[25,26] In the case of NWs, the stress might be induced by the Laplacian pressure caused by their small radius or by the excess of Boron impurities in the shell.[27,28]

As discussed, e.g., in Ref. 29, the formation of a complete monolayer (ML) slice during the VLS growth of NWs is almost instantaneous. In this case, the rate of nucleation-mediated NW growth in the [112] direction, $V = h/t_*$, where h is the height of Si ML, is determined by the waiting time t_* between two consecutive nucleation acts. While considering the ID pathway 3, we therefore assume that B atoms incorporate into the NW and diffuse along the 2D liquid-solid interface during time t_*. Such process is repeated upon the completion of each Si ML, leading to an axially homogeneous B distribution, since all MLs are identical. Time t_* can be easily estimated from the growth rate and equals 0.013 s. Putting $t = t_*$ in Eq. (6), the best fit to the experimental profile corresponds to $D = 1.56 \times 10^{-11}$ cm^2/s. This value is much larger than the solid diffusion coefficient, because the ID diffusion is 2D. On the other hand, it is much smaller than the diffusivity at the solid Si surface in contact with vapor (typically of the order of 10^{-8} cm^2/s (Ref. 30)). This also seems reasonable, because the diffusion coefficient at the solid-liquid interface should be much smaller than that on the solid-vapor interface. However, the boundary condition with a constant concentration is less easily justified for a short-scale ML growth. Overall, the ID mechanism has to be considered to account for the dopant distribution in the Si NW core, although we cannot make a definite commitment regarding its stronger contribution with respect to the VS mechanism.

In summary, we have presented the 3D mapping of B-doped Si NWs obtained by the laser-assisted APT. A convenient and an effective method to analyze the NWs by APT has been developed. It has been shown that boron is distributed inhomogeneously in the volume of Si NWs. Theoretical model has been developed that fits well the experimental dopant profile at $Dt = 20.25$ nm^2. The VS and ID mechanisms of boron incorporation have been considered, yielding the 3D solid diffusivity of B at 4.22×10^{-16} cm^2/s and the 2D diffusivity along the solid-liquid NW interface at 1.56×10^{-11} cm^2/s. We now plan to perform more APT experiments with Si NWs grown at different conditions and to model theoretically the spatial distributions of dopants incorporated by different kinetic pathways.

ACKNOWLEDGMENTS

This work was partially supported by the DGA (Direction Générale de l'Armement) of France under the Contract No. REI-N°2008.34.0031, Russian Ministry of Education and Science (Contract Nos. 02.740.11.0383, 16.740.11.0019, and 14.740.11.0592), the scientific program of Russian Academy of Sciences "Fundamental aspects of nanotechnologies and nanomaterials," few grants of Russian Foundation for Basic Research, and FP7 projects SOBONA and FUNPROBE.

[1] R. Rurali, Rev. Mod. Phys. **82**, 427 (2010).
[2] P. Xie, Y. Hu, Y. Fang, J. Huang, and C. M. Lieber, Proc. Natl. Acad. Sci. U.S.A **106**, 15254–15258 (2009).
[3] T. Xu, J. P. Nys, B. Grandidier, D. Stiévenard, Y. Coffinier, R. Boukherroub, R. Larde, E. Cadel, and P. Pareige, J. Vac. Sci. Technol. B **26**, 1960–1963 (2008).
[4] E. Koren, J. K. Hyun, U. Givan, E. R. Hemesath, L. J. Lauhon, and Y. Rosenwaks, Nano Lett. **11**, 183–187 (2011).
[5] N. Fukata, S. Ishida, S. Yokono, R. Takiguchi, J. Chen, T. Sekiguchi, and K. Murakami, Nano Lett. **11**, 651–656 (2011).
[6] R. S. Wagner and W. C. Ellis, Appl. Phys. Lett. **4**, 89–90 (1964).
[7] E. C. Garnett, Y.-C. Tseng, D. R. Khanal, J. Wu, J. Bokor, and P. Yang, Nat. Nanotechnol. **4**, 311–314 (2009).
[8] E. Koren, N. Berkovitch, and Y. Rosenwaks, Nano Lett. **10**, 1163–1167 (2010).
[9] D. E. Perea, E. R. Hemesath, E. J. Schwalbach, J. L. Lensch-Falk, P. W. Voorhees, and L. J. Lauhon, Nat. Nanotechnol. **4**, 315–319 (2009).
[10] B. P. Geiser, D. J. Larson, E. Oltman, S. Gerstl, D. Reinhard, T. F. Kelly, and T. J. Prosa, Microsc. Microanal. **15**, 292–293 (2009).
[11] B. Gault, D. Haley, F. de Geuser, M. P. Moody, E. A. Marquis, D. J. Larson, and B. P. Geiser, Ultramicroscopy **11**, 448–457 (2011).
[12] W. H. Chen, "Modeling the growth of Si nanowires and atomic scale metrology of Si nanowire composition," Ph.D. dissertation (Université de Rouen, 2011).
[13] D. E. Perea, E. Wijaya, J. L. Lensch-Falk, E. R. Hemesath, and L. J. Lauhon, J. Solid State Chem. **181**, 1642–1649 (2008).
[14] T. J. Prosa, R. Alvis, L. Tsakalakos, and V. S. Smentkowski, J. Microsc. **239**, 92–98 (2010).
[15] T. Xu, J. P. Nys, A. Addad, O. I. Lebedev, A. Urbieta, B. Salhi, M. Berthe, B. Grandidier, and D. Stiévenard, Phys. Rev. B **81**, 115403 (2010).
[16] W. H. Chen, R. Larde, E. Cadel, T. Xu, B. Grandidier, J. P. Nys, D. Stievenard, and P. Pareige, J. Appl. Phys. **107**, 084902 (2010).
[17] T. Kawashima, G. Imamura, T. Saitoh, K. Komori, M. Fujii, and S. Hayashi, J. Phys. Chem. C **111**, 15160–15165 (2007).
[18] B. Gault, M. Muller, A. La Fontaine, M. P. Moody, A. Shariq, A. Cerezo, S. P. Ringer, and G. D. W. Smith, J. Appl. Phys. **108**, 044904 (2010).
[19] C.-M. Hsu, S. T. Connor, M. X. Tang, and Y. Cui, Appl. Phys. Lett. **93**, 133109-3 (2008).
[20] E. T. Goodwin and J. Staton, Q. J. Mech. Appl. Math. **1**, 220–224 (1948).
[21] G. E. McGuire, *Semiconductor Materials and Process Technology Handbook* (Noyes Publication, 1988), pp. 501–504.
[22] N. E. B. Cowern, G. F. A. van de Walle, D. J. Gravesteijn, and C. J. Vriezema, Phys. Rev. Lett. **67**, 212–215 (1991).
[23] M. Uematsu, J. Appl. Phys. **82**, 2228–2246 (1997).

[24]D. De Salvador, E. Napolitani, S. Mirabella, G. Bisognin, G. Impellizzeri, A. Carnera, and F. Priolo, Phys. Rev. Lett. **97**, 255902 (2006).
[25]A. V. Osipov, F. Schmitt, S. A. Kukushkin, and P. Hess, Appl. Surf. Sci. **188**, 156–162 (2002).
[26]V. G. Dubrovskii, G. E. Cirlin, and V. M. Ustinov, Phys. Rev. B **68**, 075409 (2003).
[27]V. G. Dubrovskii and N. V. Sibirev, Phys. Rev. E **70**, 031604 (2004).
[28]V. Consonni, M. Hanke, M. Knelangen, L. Geelhaar, A. Trampert, and H. Riechert, Phys. Rev. B **83**, 035310 (2010).
[29]V. G. Dubrovskii, N. V. Sibirev, J. C. Harmand, and F. Glas, Phys. Rev. B **78**, 235301 (2008).
[30]D. Srivastava and B. J. Garrison, Phys. Rev. B **46**, 1472 (1992).